Implications of gate edge electric field in AlGaN/GaN high electron mobility transistors during OFF-state degradation

H. Sun*, M. Montes Bajo**, M. J. Uren, M. Kuball

Center for Device Thermography and Reliability (CDTR), H.H. Wills Physics Laboratory, University of Bristol, Bristol BS8 1TL, United Kingdom

Gate degradation in high electron mobility transistors (HEMTs) under OFF-state stress results from the high electric field near the gate edge. We investigate the evolution of this field over time in AlGaN/GaN HEMTs upon OFF-state stress using a combination of electroluminescence (EL) microscopy and spectroscopy. EL analysis suggests that the electric field at the sites of generated surface defects is lowered after the stress, with greater lowering at higher stress temperature. The ON-state EL spectrum remains unchanged after the stress, suggesting that the regions without generated defects are not affected during the degradation. A finite element model is employed to further demonstrate the effect of surface defects on the local electric field. A correlation is observed for the spatial distribution of the EL intensity before and after the generation of leakage sites, which provides a prescreening method to predict possible early failures on a device.

Key words: AlGaN/GaN high electron mobility transistor, OFF-state stress, gate leakage, electric field, electroluminescence, surface defect, electrochemical reaction

1. Introduction

GaN-based technologies have shown great promise in power and RF electronics applications. However, the reliability of GaN-based high electron mobility transistors (HEMTs) remains a major challenge. Among all reliability issues, gate degradation or breakdown has received a great deal of attention [1-9]. High electric field in OFF state may result in material changes that lead to an unrecoverable increase of gate current in AlGaN/GaN HEMTs. Such gate leakage degradation is usually accompanied by the emergence of EL "hot spots" as well as the formation of structural defects on the drain side of the gate edge [10]. The permanent increase of gate leakage is believed to result primarily from the formation of percolation conductive paths in the barrier [3-5]. Several mechanisms have been proposed to explain the formation of the structural defects including inverse piezoelectric effect [11-13], electrochemical reactions [14,15], gate metal diffusion [16,17], as well as contributions from pre-existing defects or irregularities from materials and processing such as dislocations [18] or step edges [19].

The OFF-state degradation process is electric field driven, and a step stress test with applied negative gate bias is commonly used to determine what was initially believed to be the "critical" voltage or field for gate breakdown [6,11-13]. Similar to oxide breakdown in MOSFETs, the time for a permanent increase of gate leakage current, is often referred to as the time-to-breakdown, t_{BD}. It was reported that t_{BD} is strongly field dependent, and in fact the "critical" voltage greatly varies with the time duration chosen in a step stress [1,2,7]. This is contrary to the model based on the inverse piezoelectric effect. Recent studies have demonstrated a close correlation between field-driven electrochemical reactions and OFF-state degradation [14,15,20], in line with our observations on gate degradation during the stress test, which are discussed later.

* Corresponding author. E-mail address: huarui.sun@bristol.ac.uk

** Present address: ICFO – The Institute of Photonic Sciences, 08860 Castelldefels (Barcelona), Spain.

Fig. 1 shows an example of the gate leakage current for GaN-on-SiC HEMTs stressed at a fixed negative gate bias V_{gs} = -15 V, and drain bias V_{ds} varied from 40 V to 55 V. In addition to the increase of gate leakage with V_{ds}, there is a shift of the curves to shorter times with higher V_{ds} (and thus greater gate-drain field), demonstrating the field-accelerated leakage generation. The increase in current occurs as leakage paths are continuously formed, each of which carries a few μA current. This translates to a local current density of approximately 10 mA/mm at the leakage spot, based on the average size (~100 nm) of the failure site revealed by AFM (shown later in Fig. 8). In comparison, an unstressed device under the same OFF-state bias has a finite leakage current density of ~ 10^{-2} mA/mm (see Fig. 1 at t = 1 s). The prominent increase of current density translates to a reduction of the effective local impedance at the failure sites, and hence a change in the electric field distribution in the immediate vicinity of a failure spot would be anticipated. This raises one critically interesting question: How does the electric field at the edge of the gate change upon the generation of leakage spots?

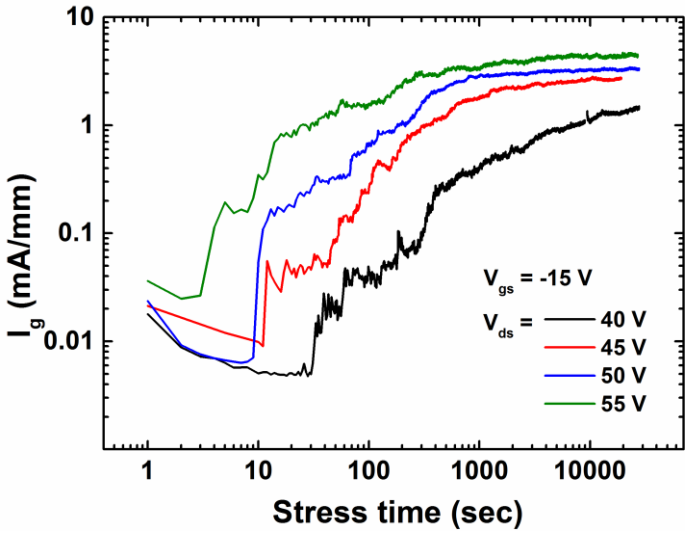

Fig. 1. Gate leakage current over time for GaN-on-SiC HEMTs stressed at V_{gs} = -15 V and V_{ds} = 40 to 55 V at room temperature.

The gate edge electric field in an AlGaN/GaN HEMT can be characterized by EL microscopy and spectroscopy. In OFF state, electrons from the gate that reach the two-dimensional electron gas (2DEG) channel may partly lose their energy by emitting visible and infrared light through intraband transitions or Bremsstrahlung [21-24]. In this paper, we demonstrate an experimental approach to characterize this electric field using EL analysis. The aim is to understand how the electric field in different regions on the gate edge changes with OFF-state stress over time, and how this field reacts to the generation of leakage paths. In addition, we explore how the field change correlates to the degree of degradation in a device under OFF-state stress. For this purpose, devices were stressed at elevated temperatures to accelerate gate leakage for enhanced degradation. Knowing the gate edge electric field distribution provides insights into the understanding of the OFF-state degradation mechanisms.

2. Experimental details

The devices studied were AlGaN/GaN HEMTs grown by metal-organic chemical vapor deposition (MOCVD) on SiC substrates. The heterostructure consisted of a 1.9 μm Fe-doped GaN buffer layer and a 25 nm $Al_{0.25}Ga_{0.75}N$ barrier layer. Standard TiAlTiAu Ohmic contact was used for the source and drain electrodes, and standard NiAu Schottky contact was used for the gate electrode. The nominal gate length, source-drain gap, and source-to-gate distance, were 0.6 μm, 4 μm, and 1 μm, respectively. The AlGaN/GaN HEMTs were passivated with a $SiN_x/SiO_2/SiN_x$ multilayer and isolated

by mesa etching. The devices were stressed for about 7.5 hours in OFF-state conditions at a gate bias V_{gs} = -15 V (pinch-off voltage V_{po} = -5 V) and drain bias V_{ds} in a range from 40 V to 55 V. In one specific set of tests, four identical devices were stressed under the same OFF-state bias (V_{gs} = -15 V, V_{ds} = 40 V) with a heat sink temperature varied from 21 ˚C to 120 ˚C. Over the entire course of the stress experiment, the gate current, I_g, was monitored and EL images were continuously captured using a Peltier-cooled 16-bit monochrome charge coupled device (CCD) attached to a microscope. Optical spectra from ON-state EL were obtained before and after the stress using a grating spectrometer covering visible and near-infrared bands, and OFF-state EL spectra were recorded after the stress. The GaN-on-SiC devices tested have a dislocation density of ~ 10^9 cm^{-2}; for comparison, a similar stress stress test (V_{gs} = -15 V, V_{ds} = 40 V, room temperature) was performed on a GaN-on-GaN HEMT with a significantly lower dislocation density of ~ 10^5 cm^{-2} (the details of this device can be found in [25]).

3. Results and discussion

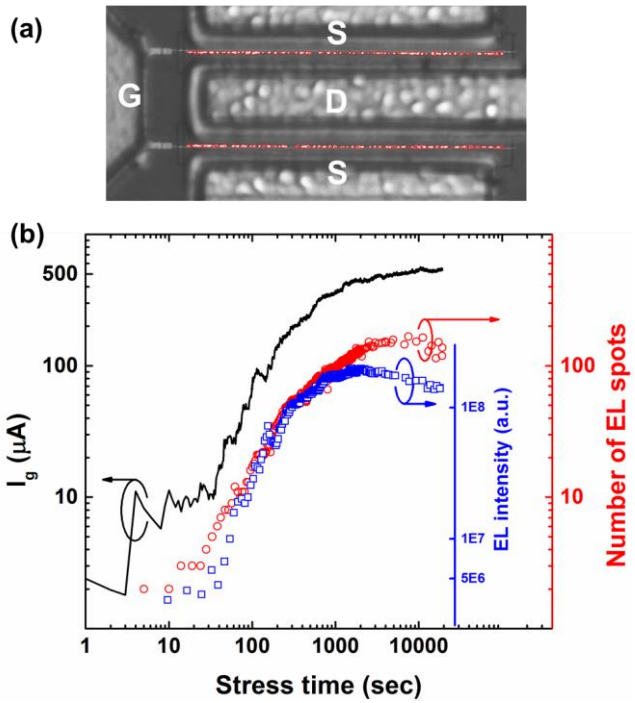

Fig. 2. (a) False color EL image of a 2×100 μm GaN-on-SiC HEMT after 7.5 hours stress at V_{gs} = -15 V and V_{ds} = 45 V at room temperature. (b) Gate leakage current, number of EL "hot spots", and total EL intensity as a function of stress time.

A typical EL image of a 2×100 μm HEMT (overlaid with the transistor image) is shown in Fig. 2(a), with discrete EL "hot spots" illustrating the formation of local gate leakage sites. The number of EL spots increases over time until it reaches a plateau (> 2000 s). From that point onwards the total EL intensity experiences a gradual decay. This saturation regime is also seen in the reduced slope of the gate current increase. The saturation in failure spot generation was primarily attributed to the limited supply of electrochemically active species on the device surface needed in the degradation process [20], although contributions from pre-existing defects such as point defects or dislocations may also be possible. However, as shown in Fig. 3, the GaN-on-GaN device shows a similar trend in both the gate current leakage and the number of EL "hot spots" over time, with a generated EL spot density of ~ 1 per μm gate width, comparable to that of a GaN-on-SiC device (Fig. 2). These two devices significantly differ in their dislocation density and processing condition, which suggests that pre-existing defects in materials or from processing are not likely the primary cause of the saturation of failure site formation.

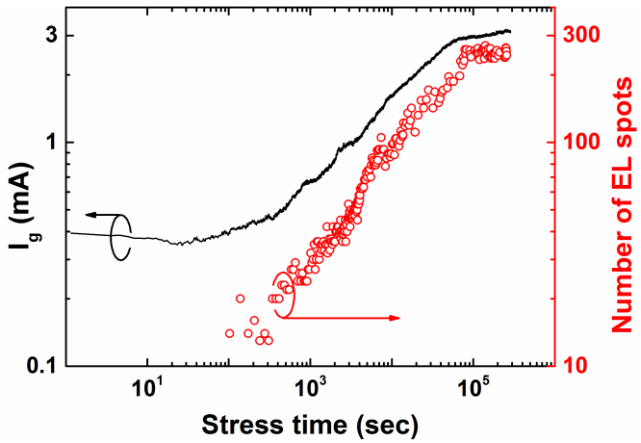

Fig. 3. Gate leakage current and number of EL "hot spots" over time for a GaN-on-GaN HEMT stressed at V_{gs} = -15 V and V_{ds} = 40 V at room temperature.

Figs. 4(a)-(c) show the gate leakage current, the number of EL "hot spots", and the total EL intensity over time for devices stressed at different temperatures. It is evident that the OFF-state degradation is a temperature-accelerated process, with curves shifted to shorter times at elevated temperatures. The insets of Fig. 4(a) and Fig. 4(b) show the Arrhenius relation between temperature and the characteristic time τ (defined as the time for 63.2% of the failure spots to appear) for the gate current and the number of EL spots, from which an activation energy of 0.42 eV and 0.44 eV for the two processes was extracted, respectively. The nearly identical activation energies again demonstrate that the generation of EL "hot spots" and the formation of leakage paths are tied to the same process. Interestingly, the gate current for the device stressed at 120 °C starts to decrease after 3000 s; a reduction in this saturation regime is more noticeable in the EL intensity. This is likely linked to the changes in the electric field at the leakage sites, which is discussed next.

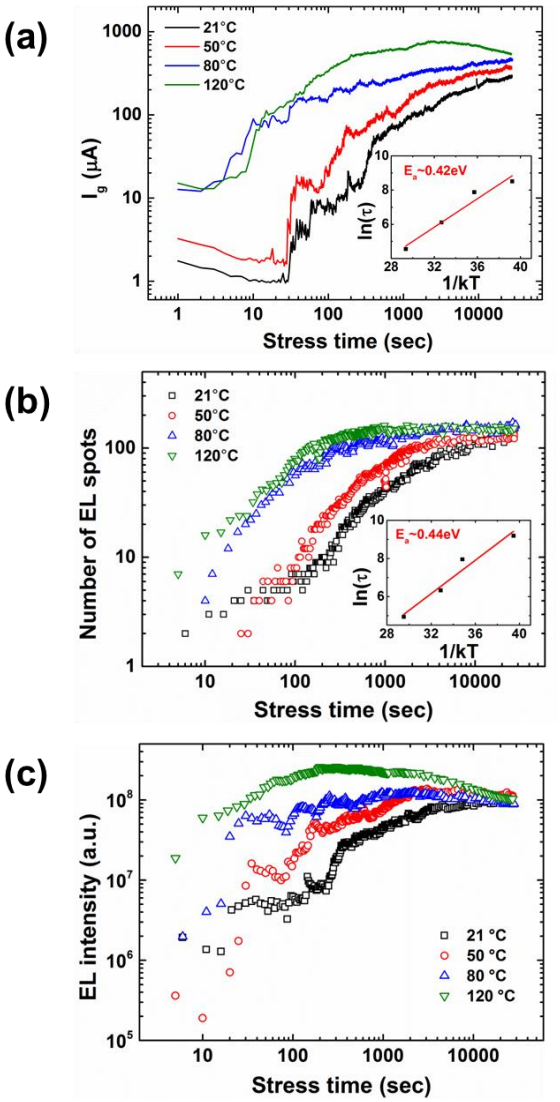

Fig. 4. (a) Gate leakage current, (b) number of EL "hot spots", and (c) total EL intensity over time for GaN-on-SiC HEMTs stressed at V_{gs} = -15 V and V_{ds} = 40 V at different temperatures. The Arrhenius plot for gate current and generation of EL spots is shown as an inset of Fig. 4(a) and Fig. 4(b), respectively.

In the presence of OFF-state bias and thus high gate-drain electric field, the generated conductive paths on the gate edge allow electrons to leak through the AlGaN barrier into the device channel which are then accelerated towards the drain. These hot electrons relax their high kinetic energy via intraband transitions or Bremsstrahlung, leading to broadband EL emission [21-24]. In theory, the amplitude of the EL signal is determined by both the current carried by the hot electrons and the magnitude of the electric field in which these electrons are accelerated. The current represents the amount of hot electrons and the field decides the probability of these electrons to emit light. The ratio of the EL intensity and the current, therefore, is expected to be a qualitative measure of the electric field [26,27]. Fig. 5 plots the EL intensity/I_g ratio as a function of time for all devices. The initial fluctuation at the beginning of stress (< 100 s) is due to the appearance of the first couple of EL hot spots accompanied by the rapid changes in both gate leakage current and EL intensity. After 100 s the uncertainty reduces and the EL intensity/I_g ratio experiences a steady decay over time, indicating a gradual drop in the electric field at the "hot spots". Similar behavior in ON-state hot electron degradation was reported in Refs. 26 and 27. It should be noted that the EL intensity/I_g ratio only describes the field at the failure spots but not in intact areas in between them that are not light emitting. Furthermore, the differences in the absolute magnitude of EL intensity/I_g ratio between different

temperatures may not accurately represent the actual differences in the corresponding electric field, since the strength of EL emission is strongly temperature dependent [22].

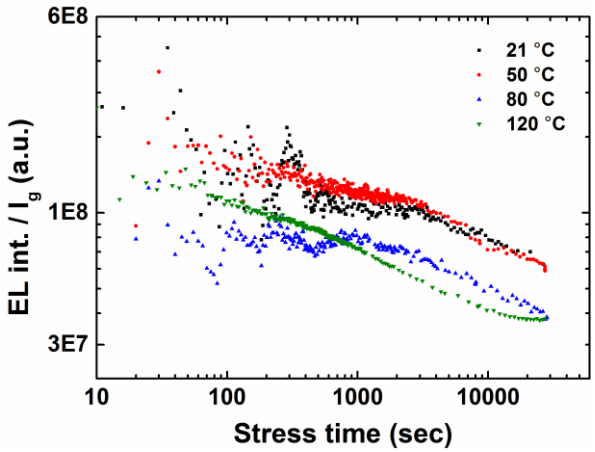

Fig. 5. Ratio of EL intensity and gate leakage current over time for GaN-on-SiC devices stressed at different temperatures.

To confirm this change in field, the optical spectrum from the EL "hot spots" was recorded. Hot electron temperature obtained from the high energy tail of the broadband EL spectrum provides a measure of the electric field at the emission sites. Fig. 6 shows the EL spectrum (measured at V_{gs} = -15 V, V_{ds} = 40 V at room temperature) and its corresponding hot electron temperature for devices stressed for 7.5 hours at different temperatures. For comparison, a monitor device was stressed at 21 ˚C for 10 minutes until only 20 EL spots appeared (red circle). The device stressed at 21 ˚C for 7.5 hours has lower electron temperature than the monitor device, suggesting that the electric field is lowered over time during the stress, consistent with the decaying EL intensity/I_g ratio shown in Fig. 5. This is possibly related to the build-up of traps in forming the conductive paths in the AlGaN layer [28], reducing effectively the local impedance at the failure sites from the device top surface to the channel as the degradation progresses. The degree of this field lowering increases with stress temperature, which is sensible since the degradation is temperature accelerated, as illustrated in Fig. 4. In this sense, the OFF-state EL spectrum offers a quantitative means to assess the degree of degradation.

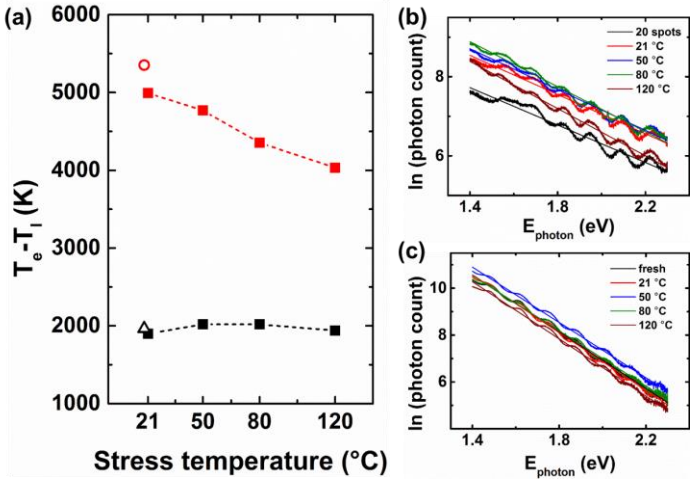

Fig. 6. (a) Hot electron temperature relative to lattice temperature (T_e-T_l) in OFF state (red squares) and ON state (black squares) derived from (b) and (c). The red circle represents the monitor device stressed for 10 minutes with only 20 EL "hot spots" generated. The black triangle represents the unstressed device measured in ON state for comparison. (b) Optical spectra from EL spots measured in OFF state (V_{gs} = -15 V and V_{ds} = 40 V) at room temperature. (c) EL spectra measured in ON state (V_{gs} = 0 V and V_{ds} = 20 V) at room temperature.

Knowing that the emissive leakage spots have a falling field during stress, a natural question follows immediately: what happens to the field in regions at the edge of the gate where failure sites are not generated? This is important since this field is the primary driving force for the degradation, determining how fast new failure sites would be generated. However, OFF-state EL measurement is not able to directly capture the electric field in these unaffected areas since light is only emitted from the defect sites through gate leakage. We instead look at the ON-state EL profile and spectrum to see if there are any changes from the stress in the unaltered areas at the edge of the gate. In ON-state conditions (e.g., V_{gs} = 0 V, V_{ds} = 20 V), EL is expected to form a continuous line along the gate finger for an unstressed device (Fig. 7 top, Image A). However, as a result of the OFF-state stress, a device with generated "hot spots" shows dark spots in its ON-state EL image, which can be seen in the discontinuous EL line profile (Fig. 7 top, Image C). These dark spots appear only at the locations of the stress-induced "hot spots" (Fig. 7 top, Image B). Fig. 7 bottom plots the OFF-state EL intensity of the stressed device together with the ratio of ON-state EL after and before the stress. The dips in the device's ON-state EL profile align precisely with the peaks in its OFF-state EL profile. This may be due to the non-radiative defect states in the AlGaN device layer induced during the degradation [29]. Alternatively, the leakage sites may have locally lowered barrier and correspondingly reduced 2DEG concentration, leading to a reduction in ON-state EL intensity. However, this seems less likely since the drain current does not show apparent degradation after the stress (not shown here).

The ON-state EL shows rather constant intensity in unaltered regions (Fig. 7 top, Image C), and the ratio of EL intensity after and before the stress is approximately one in areas outside the "hot spots" (Fig. 7 bottom), which implies that these regions are not influenced by the stress. The inhomogeneous EL distribution of a stressed device also means that the EL intensity measured in ON state is primarily from regions without failure sites, so it is sensible to estimate the change of field after stress in these unaltered areas using the ON-state EL spectrum. Fig. 6(c) shows the ON-state EL spectra for all devices after the OFF-state stress. Contrary to the EL spectrum recorded in OFF state, the ON-state EL spectrum shows no apparent variations among all devices. The hot electron temperature remains constant for either a fresh device or devices stressed at different temperatures (Fig. 6(a), black triangle and squares). Although the ON-state EL does not represent the actual electric field during the OFF-state stress, it provides evidence that the regions without failure sites are not affected by the stress. An unchanged field in the unaltered areas would imply a constant external force that drives the degradation, which is expected to result in a fixed rate of EL spot generation. This could well explain the nearly constant slope in the central region of the curve of the EL spot generation (Figs. 2, 3 and 4 (b)).

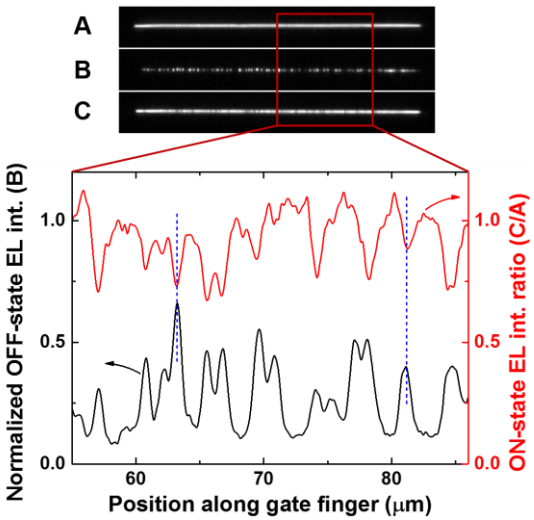

Fig. 7. Top: (A) ON-state EL image of an unstressed 100 μm wide GaN-on-SiC device recorded at V_{gs} = 0 V and V_{ds} = 20 V. (B) OFF-state EL image of the same device after stress at V_{gs} = -15 V and V_{ds} = 40 V. (C) ON-state EL image of the device after stress recorded at V_{gs} = 0 V and V_{ds} = 20 V. Bottom: Normalized OFF-state EL profile of the stressed device (black curve, taken from Image B) and the ratio of ON-state EL after and before stress (red curve).

After the stress and EL tests, the passivation layer was etched away in 1:10 HF:H_2O; the source and drain contacts and gate metals were then removed using aqua regia, followed by a surface cleaning with piranha solution (see detailed procedure in Ref. 30). The source-drain gap on each device was then scanned using an atomic force microscope (AFM). Fig. 8(a) shows the gate regions for devices stressed at different temperatures, revealing surface pits associated with the generation of "hot spot" leakage sites. These surface pits are most likely the imprints of new species formed via electrochemical reactions [14,20]. It is evident that the specific morphology of the surface pit defects varies with the stress temperature (Fig. 8(b)). For example, the average size of pits in the direction parallel to the gate width increases with temperature whereas that in the direction normal to the gate width reduces with temperature. This is probably linked to the specific location of barrier lowering in the electrochemical breakdown process that forms the pits. Unlike the distinct temperature dependence of the pit size in either direction, the geometric mean of the two dimensions, which links to the average area of a pit, is only weakly dependent on temperature. This is consistent with the above-mentioned self-limiting mechanism involving the consumption of surface mobile species that are electrochemically active, which leads to the saturation of defect generation [20].

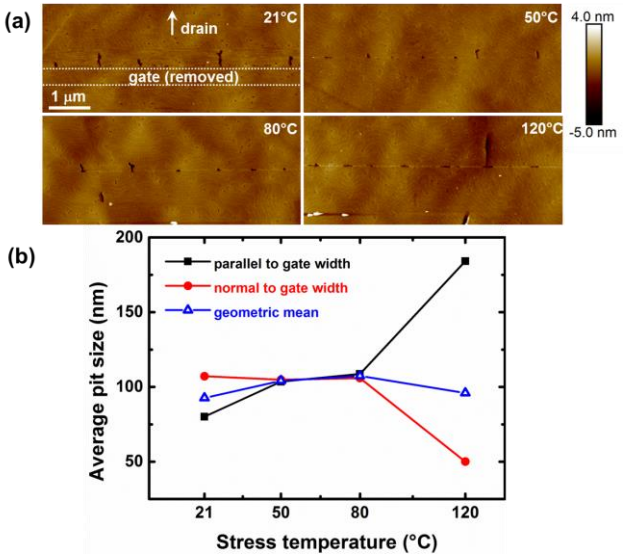

Fig. 8. (a) AFM images of AlGaN surface near the gate after removal of passivation and metals. The original gate and drain locations are marked. (b) Average size of surface pits in the direction parallel (black) and normal (red) to the gate width and geometric mean of the two dimensions (blue).

To help understand the degradation-induced changes in the electric field, a 3D finite element model in ANSYS was employed to estimate the field at the gate edge with added surface defects. It should be noted that the following assumptions made in the simulation are sensible yet not rigorous, since the detailed shapes and physical properties of the surface defects are not known. In reality, the generated surface defects may have complex structures and non-uniform electrical properties, and a detailed description falls beyond the scope of this work. The finite element model was validated by comparing the calculated profile of cross-sectional electric field in between defects with the result from a 2D drift diffusion model using Silvaco ATLAS. The OFF-state two-dimensional electron gas (2DEG) was approximated in the finite element model by two thin metal sheets in contact with the source and drain, respectively, with a gap in between corresponding to the depletion region at the gate edge in the gate-drain gap. This is based on the cross-sectional distribution of electron concentration calculated using the ATLAS model. The defects were approximated by thin bodies with lower resistivity at the device surface in contact with the gate. The leakage path between the surface and the 2DEG was assumed to have such high effective impedance that it had little impact on the field. Two types of surface defects were considered (Fig. 9 top): one that appears perpendicular to the gate width

(representative of room temperature, Fig. 8(a)) and one that stretches along the width (representative of high temperature, Fig. 8(a)).

As shown in Fig. 9 (bottom), the area near the tip of a defect (Spots 1 and 2) has enhanced field due to the small radius of curvature and its proximity to the drain. It appears that the new "gate edge" moves to the tip of the defect, screening the field at the original gate edge inside the defect. This illustrates the growth of the surface pit defects in the field-driven electrochemical breakdown process, as seen in the AFM images (Fig. 8(a)). Field intensification near the end of a pit triggers the lowering of the barrier and the transport of the surface mobile species, promoting the local electrochemical reactions. This is consistent with the observed fine structures at the end of a surface pit (Fig. 8(a)), which are commonly observed in electrochemical breakdown processes in porous silicon [31]. It is worth noting that the gate edge field outside the defects (Spot 3) is unchanged with respect to the unperturbed value (field without any defects). This is consistent with the obtained constant electron temperature in Fig. 6(a), which again suggests that the saturation of defect generation at long stress times is not primarily caused by the field. It requires an additional self-limiting mechanism such as a limited supply of the mobile species needed for the electrochemical reactions at the surface pits [20].

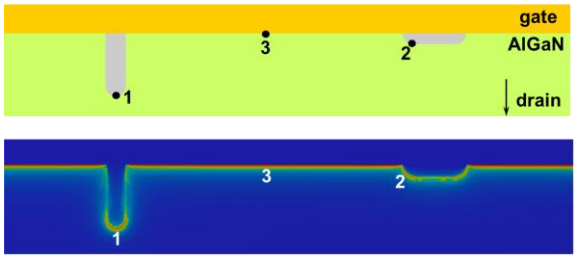

Fig. 9. Top: Plane view of the simulated structure in the finite element model. Bottom: 2D contour plot of the calculated electric field near the gate edge at the AlGaN/SiN_x interface (V_{gs} = -15 V and V_{ds} = 40 V). Spots 1 and 2 at the tip of the defects have intensified field due to their small radius of curvature and proximity to the drain. The field at Spot 3 at the edge of the gate is not affected by the added surface defects.

Given the discrete and chronological behavior of the emergence of "hot spot" leakage paths, it is reasonable to assume degradation starts from the weakest or most vulnerable spots at the edge of the gate. An initially inhomogeneous distribution of electric field under reverse bias may be present due to crystallographic irregularities or gate edge roughness. This results in a non-uniform distribution of initial leakage current density, which is demonstrated in the EL line profile of a moderately biased (V_{gs} = -15 V, V_{ds} = 30 V) device before the permanent increase of gate current (black curve in Fig. 10). The device was then stressed at V_{gs} = -15 V, V_{ds} = 50 V until several "hot spots" were generated, as illustrated in the EL line profile (red curve). A great percentage of the peaks on the black curve align with the positions of the generated "hot spots" on the red curve. Statistically, spots with high initial current density fail first when submitted to OFF-state stress, although there is not exactly a one-to-one match, indicating a potentially more complicated relationship or other initial failure contributions. As the degradation progresses, failure sites continue to emerge from the rest of the areas, and this process continues until the defect generation reaches saturation. The final number of generated defects is not limited by the peaks in the initial EL intensity (black curve in Fig. 10) but by other self-limiting processes such as electrochemical degradation. We note that similar initial EL spatial variations in unstressed devices were also observed on a variety of transistors of different technologies, including HEMTs from commercial sources. For this reason, such EL analysis could potentially be an effective tool for wafer prescreening as it enables the prediction of early failure positions on a device.

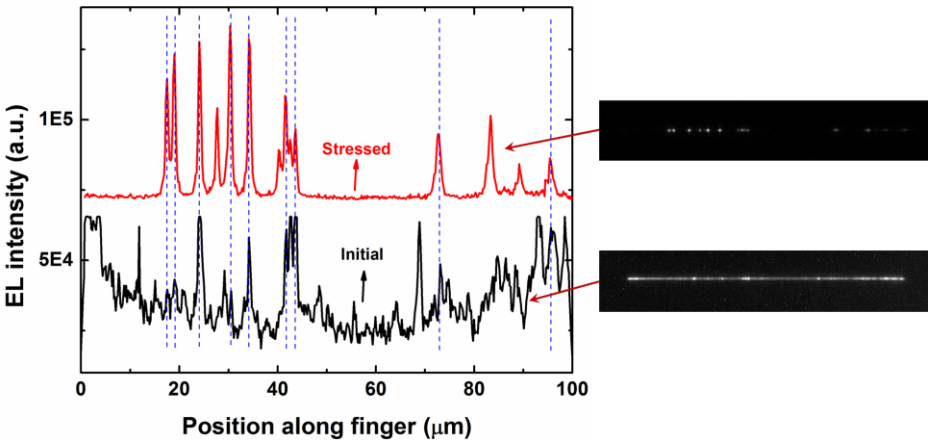

Fig. 10. Black curve: Initial EL profile before the generation of EL hot spots measured at V_{gs} = -15 V and V_{ds} = 30 V with a camera exposure time of 120 s. Red curve: EL profile after the generation of EL hot spots measured at V_{gs} = -15 V, V_{ds} = 50 V with a camera exposure time of 1 s. A vertical offset is added to the red curve to separate the two EL profiles for visual comparison. The camera exposure times were purposely chosen so that the two curves have comparable scales of EL intensity. Corresponding EL images are shown on the right.

4. Conclusions

The change of gate edge electric field has been probed using a combination of EL microscopy and spectroscopy. The field at the generated leakage sites lowers over time, with greater lowering at higher stress temperature. The ON-state EL spectrum suggests that the non-leaky regions are not affected by the stress, which is supported by the finite element model. This is strong evidence that the observed saturation of defect generation is not primarily limited by the electric field. It has been demonstrated that EL analysis can be used as an effective approach for locating potential early failure spots on a device.

Acknowledgements

The authors thank A. Murray (University of Bristol) for passivation and metals removal from the devices, and J. Anaya Calvo, M. Caesar, C. Hodges, J. W. Pomeroy, and N. Vasiljevic (University of Bristol) for helpful discussions. The GaN-on-SiC devices were provided by QinetiQ Ltd. under support from the UK Ministry of Defence. The GaN-on-GaN devices were provided by Air Force Research Laboratory (J. Blevins). This work was supported by EPSRC under Grants EP/K024345/1 & EP/L007010/1 & EP/K014471/1.

References

[1] D. Marcon, T. Kauerauf, F. Medjdoub, J. Das, M. Van Hove, P. Srivastava, K. Cheng, M. Leys, R. Mertens, S. Decoutere, G. Meneghesso, E. Zanoni, and G. Borghs, *Proc. IEEE IEDM*, 20.3.1 (2010).
[2] D. Marcon, G. Meneghesso, T.-L. Wu, S. Stoffels, M. Meneghini, E. Zanoni, and S. Decoutere, *IEEE Trans. Electron Device* 60, 3132 (2013).
[3] E. Zanoni, M. Meneghini, A. Chini, D. Marcon, and G. Meneghesso, *IEEE Tran. Electron Devices.* 60, 3119 (2013).
[4] D. J. Cheney, E. A. Douglas, L. Liu, C. F. Lo., Y. Y. Xi., B. P. Gila, F. Ren, D. Horton, M. E. Law, D. J. Smith, and S. J. Pearton, *Semicond. Sci. Technol.* 28, 074019 (2013).
[5] D. A. Cullen, D. J. Smith, A. Passaseo, V. Tasco, A. Stocco, M. Meneghini, G. Meneghesso, and E. Zanoni, *IEEE Trans. Device Mater. Reliab.* 13, 126 (2013).
[6] E. A. Douglas, C. Y. Chang, B. P. Gila, M. R. Holzworth, K. S. Jones, L. Liu, Jinhyung Kim, Soohwan Jang, G. D. Via, F. Ren, S. J. Pearton, *Microelectron. Reliab.* 52, 23 (2012).
[7] D. Marcon, J. Viaene, P. Favia, H. Bender, X. Kang, S. Lenci, S. Stoffels, S. Decoutere, *Microelectron. Reliab.* 52, 2188 (2012).
[8] M. Meneghini, A. Stocco, M. Bertin, D. Marcon, A. Chini, G. Meneghesso, and E. Zanoni, *Appl. Phys. Lett.* 100, 033505 (2012).
[9] L. Brunel, B. Lambert, P. Mezenge, J. Bataille, D. Floriot, J. Grünenpütt, H. Blanck, D. Carisetti, Y. Gourdel, N. Malbert, A. Curutchet, and N. Labat, *Microelectron. Reliab.* 53, 1450 (2013).

[10] M. Montes Bajo, C. Hodges, M. J. Uren, and M. Kuball, *Appl. Phys. Lett.* 101, 033508 (2012).
[11] J. Joh and J. A. del Álamo, *IEEE Electron Device Lett.* 29, 287 (2008).
[12] J. Joh, F. Gao, T. Palacios, and J.A. del Álamo, *Microelectron. Reliab.* 50, 767 (2010).
[13] J. Joh, J.A. del Álamo, K. Langworthy, S. Xie, and T. Zheleva, *Microelectron. Reliab.* 51, 201 (2011).
[14] F. Gao, B. Lu, L. Li, S. Kaun, J. S. Speck, C. V. Thompson, and T. Palacios, *Appl. Phys. Lett.* 99, 223506 (2011).
[15] F. Gao, S.-C. Tan, J. A. del Álamo, C. V. Thompson, and T. Palacios, *IEEE Trans. Electron Device* 61, 437 (2014).
[16] S. D. Burnham, R. Bowen, P. Willadsen, H. Bracamontes, P. Hashimoto, M. Hu, D. Wong, M. Chen, and M. Micovic, *Phys. Status Solidi C* 8, 2399 (2011).
[17] M. R. Holzworth, N. G. Rudawski, P. G. Whiting, S. J. Pearton, K. S. Jones, L. Lu, T. S. Kang, F. Ren, E. Patrick, and M. E. Law, *Appl. Phys. Lett.* 103, 023503 (2013).
[18] M. Ťapajna, S.W. Kaun, M. H. Wong, F. Gao, T. Palacios, U. K. Mishra, J. S. Speck, and M. Kuball, *Appl. Phys. Lett.* 99, 223501 (2011).
[19] N. Killat, M. Montes Bajo, T. Paskova, K. R. Evans, J. Leach, X. Li, Ü. Özgür, H. Morkoç, K. D. Chabak, A. Crespo, J. K. Gillespie, R. Fitch, M. Kossler, D. E. Walker, M. Trejo, G. D. Via, J. D. Blevins, and M. Kuball, *Appl. Phys. Lett.* 103, 193507 (2013).
[20] M. Montes Bajo, H. Sun, M. J. Uren, and M. Kuball, *Appl. Phys. Lett.* 104, 223506 (2014).
[21] N. Shigekawa, K. Shiojima, and T. Suemitsu, *Appl. Phys. Lett.* 79, 1196 (2001).
[22] N. Shigekawa, K. Shiojima, and T. Suemitsu, *J. App. Phys.* 92, 531 (2002).
[23] M. Ťapajna, R. J. T. Simms, Y. Pei, U. K. Mishra, and Martin Kuball, *IEEE Electron Device Lett.* 31, 662 (2010).
[24] M. Meneghini, A. Stocco, N. Ronchi, F. Rossi, G. Salviati, G. Meneghesso, and E. Zanoni, *Appl. Phys. Lett.* 97, 063508 (2010).
[25] T. Paskova, D. A. Hanser, and K. R. Evans, *Proc. IEEE* 98, 1324 (2010).
[26] M. Meneghini, G. Meneghesso, and E. Zanoni, *IEEE Trans. Device Mater. Reliab.* 13, 357 (2013).
[27] M. Meneghini, A. Stocco, R. Silvestri, G. Meneghesso, and E. Zanoni, *Appl. Phys. Lett.* 100, 233508 (2012).
[28] M. Silvestri, M. J. Uren, N. Killat, D. Marcon, and M. Kuball, *Appl. Phys. Lett.* 103, 043506 (2013)
[29] C. Hodges, N. Killat, S. W. Kaun, M. H. Wong, F. Gao, T. Palacios, U. K. Mishra, J. S. Speck, D. Wolverson, and M. Kuball, *Appl. Phys. Lett.* 100, 112106 (2012).
[30] P. Makaram, J. Joh, J. A. Del Álamo, T. Palacios, and C. V. Thompson, *Appl. Phys. Lett.* 96, 233509 (2010).
[31] M. I. J. Beale, J. D. Benjamin, M. J. Uren, N. G. Chew, and A. G. Cullis, *J. Crystal Growth* 73, 622 (1985).